Multilevel-Coded QAM With MIMO Turbo-Equalization in Broadband Single-Carrier Signaling

Kimmo Kansanen, *Member, IEEE*, Christian Schneider, Tad Matsumoto, *Senior Member, IEEE*, and Reiner Thomä, *Senior Member, IEEE*

***Abstract*—A new scheme employing multilevel coded bit-interleaved transmission allowing for efficient turbo-equalization is proposed for multiple-input–multiple-output (MIMO) broadband single-carrier signaling. The proposed scheme is based on block-partitioned hierarchical constellations and offers robustness in data throughput efficiency against varying spatio-temporal characteristics of fading channels. The proposed scheme is compared to a standard bit-interleaved-coded-modulation (BICM) system in frequency-selective channels, and found to offer better overall throughput. It is also shown that level-wise retransmission control with the proposed multilevel single-carrier signaling scheme can offer further throughput improvement. Channel measurement-based simulations are used to evaluate performances of both schemes in real fields. Channel parameter analysis using a superresolution technique is performed to clarify the underlying reasons for the performance characteristics of the systems.**

***Index Terms*—Automatic repeat-request, bit-interleaved modulation, multilevel coding, multiple-input–multiple-output (MIMO) systems, throughput efficiency, turbo equalization.**

I. Introduction

EQUALIZATION of severely frequency-selective broadband channels has long been an active field of research. Turbo-equalization techniques [1] and especially suboptimal versions thereof have been known to achieve excellent performances without requiring excessive computational effort. In this paper, we concentrate on the particular turbo equalization algorithm presented in [2]–[4] for broadband single-carrier signaling. Our focus is especially on the application of the algorithm in bandwidth efficient packet-switched communications over turbo-equalized broadband channels, as future systems have to be more optimized toward packet-based transmission. The original suboptimal algorithms [2]–[4] for turbo-equalization consist of soft interference cancellation with symbol estimates computed using channel decoder feedback, followed by linear time-variant MMSE filtering and soft symbol demapping. The original algorithm is extended to bandwidth-efficient modulations, in particular bit-interleaved coded modulation [5] (BICM), in [6]. In this paper, we refer to the original algorithm as soft cancellation and MMSE filtering turbo equalization (SC/MMSE). The SC/MMSE approach differs in detector scheduling and filter coefficient computation from the space-time decision feedback (ST-DFE) algorithm presented in [7], where user ordering and serial cancellation are utilized with user-wise feed-forward and -back filters computed assuming perfect *a priori* information.

The good performance offered by receivers employing turbo detection methods relies on the successful convergence of the detector. In [6], the convergence properties of the SC/MMSE equalizer with multilevel modulated transmissions were shown to depend heavily on the symbol mapping rule used and the channel realization. In multiple-input multiple-output (MIMO) systems with more than one transmit and receive antennas [8], the convergence and the performance of the receiver depends further on the spatio-temporal structure of the propagation channel [9]. In particular, channel conditions with rich multipath scattering are often beneficial to performances of MIMO transmission techniques. In realistic channels where the spatio-temporal structure can vary significantly, transmission schemes robust against such variations are desirable.

In this paper, we study multilevel coded [10] QAM as a transmission method to achieve robustness in transmission over fading multipath channels. Similar hierarchical constellations have been proposed for transmission over fading channels in [11]. The fundamental idea of the proposed transmission method, which is related to superposition coding [12], is to construct the constellation through a combination of simpler component constellations, which are then super-positioned to form the final transmitted symbols. The unequal error protection (UEP) provided by the modulation [13], [14] is then exploited to offer adaptive throughput in varying channel conditions without explicit adjustment of the modulation format. The original proposal in [10] for decoding of multilevel codes is based on multistage techniques while recently iterative decoding methods have been proposed [15], [16] to enhance the decoding performance and reduce error propagation between the decoders. In certain cases [17] multilevel constructions can enable efficient equalization algorithms with good convergence properties to be designed. The UEP capability of the coding and modulation is translated into convergence properties of the turbo-equalizer. Earlier work on the turbo-equalization of multilevel codes can be found, e.g., in [18], where an

Manuscript received January 9, 2004, revised August 5, 2004 and November 13, 2004. This work was supported in part by TEKES, the Finnish Technology Agency, Finnish Defence Forces, Elektrobit, Instrumentointi, Nokia, and the German Federal Ministry of Education, Science Research and Technology under the HyEff project line. The review of this paper was coordinated by Dr. M. Valenti.

K. Kansanen and T. Matsumoto are with the University of Oulu, Oulu 90014, Finland (e-mail: kimmo.kansanen@ee.oulu.fi).

C. Schneider and R. Thomä are with the Ilmenau University of Technology, PSF 100 565, Ilmenau D-98684, Germany.

Digital Object Identifier 10.1109/TVT.2005.844663

adaptive decision feedback equalizer (DFE) with re-encoded symbols from the decoder is utilized. Turbo equalization of multilevel modulations is studied also e.g., in [19], where the max-log-MAP algorithm is utilized for equalization.

The transmission scheme proposed in this paper uses hierarchical block-partitioned (BP) mapping for multilevel coded symbols, where the role of the mapping is to produce a complex linear combination of BPSK modulated and interleaved bits. In the sequel, we denote the scheme as multilevel bit-interleaved coded modulation (MLBICM). A simple turbo equalizer exploiting the linearity of the symbol mapper is developed based on the sub-optimal algorithm presented in [3], [4], [6]. As a positive side-effect, the symbol-to-bit soft demapping generally required in equalization of high-order modulations [6] can be avoided. The multiple coded levels can be decoded in parallel without the interdecoder information exchange of multistage decoders, which simplifies the receiver architecture. The parallelism is partly due to the decoupling of the in-phase and quadrature components [13], [14], and partly due to the decoupling of multilevel outputs computed by the equalizer. The proposed multilevel coded scheme is compared to BICM, which is turbo-equalized with the algorithm shown in [6] and demapped with *a priori* information in a similar manner to the iterative decoding technique for BICM shown in [20]. The reference scheme is selected to emphasize the importance of suitable design of coding and modulation for turbo equalization.

A multilevel coded transmission can be designed according to a number of different principles [21] based on the symbol mapping rule used. In general the objective is to reach a desired operating point with all coding levels simultaneously by the selection or design of suitable codes for different levels. For the purpose of simplicity, however, our approach is to utilize the same code for all levels and complement the unequal error protection with a suitable automatic repeat request (ARQ) scheme. We explore the separation of ARQ processes of MLBICM coding levels to exploit the modulation's UEP capability more effectively than what is possible with a single ARQ process. We then verify the usefulness of such a pragmatic approach in realistic channel conditions.

Up to the latest standards, those designing new systems have had access to relatively accurate channel models which encapsulate the essential characteristics of the propagation channel, and model-based propagation channels have been used for link- and system-level simulations. With the introduction of MIMO transmission methods, spatio-temporal characteristics of the propagation channel have become essential in the evaluation of system performances. Accurate channel modeling has more to give to system design than ever before, but at the same time channel models have become increasingly complex. Given this situation, testing with measured channel response data can provide a realistic view of the merits and demerits of different systems. If the simulation results are combined with multipath propagation characteristics identified by the means of high resolution parameter estimation [22]–[25] and channel analysis, further insights on system behavior in the real field can be obtained. Link level performances with a MIMO setup have been studied in real fields in, e.g., [26], [9]. A goal of this paper is to correlate performance tendencies, obtained as a result of measurement data-based simulations, with the spatio-temporal characteristics estimated by using the same measurement data. This should bring us insightful information and better understanding of performances of the studied systems in varying channel conditions.

This paper is organized as follows. The system model is presented in Section II. Equalization of BICM with the SC/MMSE turbo equalizer is first presented in Section III, and the modification of the algorithm for the proposed multilevel coded system in Section IV. The performances of the the standard BICM and the proposed MLBICM schemes are studied through channel model-based simulations in Section V. Channel measurements and their usage for measurement-based simulations are detailed in Section VI, where the throughput efficiencies offered by the two schemes are presented. Comparisons are then made to illustrate the differences in the throughput behavior between the two schemes in varying spatio-temporal channel conditions. A further throughput improvement achieved through suitable ARQ design is presented. Some shortcomings and potential open issues relating to the proposed scheme are discussed in Section VII. The paper is concluded with a summary.

II. System Model

We begin by defining the multiantenna transmission method used in Section II-A. We then proceed by briefly presenting the BICM coding and modulation in Section II-B and the construction of the proposed MLBICM coding and modulation in Section II-C. A linear system model describing the received signal is presented in Section II-D. In this paper, an estimate is indicated by hat ($\hat{\cdot}$), and an underscore ($\underline{\cdot}$) is used to make a MLBICM variable distinct from a BICM variable with the same function.

A. Multiantenna Transmission

The transmission uses a layered [27] approach, where signals transmitted through different transmit antennas are encoded separately. In the transmitter, source bits are serial-to-parallel converted before being forwarded to the K antennas for the antenna-specific encoding and modulation.

B. BICM Coding and Modulation

Information bits to be transmitted through the kth antenna ($k = 1 \dots K$) are channel encoded and randomly interleaved as depicted in Fig. 1. The resulting sequence is segmented into groups of M bits each and the segments used for constructing each of the N transmitted symbols in a frame. The segmented bits for each frame can be expressed in a vector form as

$$\mathbf{b} = [\mathbf{b}^{\mathrm{T}}(1), \dots, \mathbf{b}^{\mathrm{T}}(n), \dots, \mathbf{b}^{\mathrm{T}}(N)]^{\mathrm{T}} \tag{1}$$

where the bits transmitted at the time instant $n = 1 \dots N$ through K transmit antennas are given by

$$\mathbf{b}(n) = \left[\mathbf{b}_1^{\mathrm{T}}(n), \dots, \mathbf{b}_k^{\mathrm{T}}(n), \dots, \mathbf{b}_K^{\mathrm{T}}(n)\right]^{\mathrm{T}} \tag{2}$$

with each segment $\mathbf{b}_k(n)$ of M bits for antenna k given by

$$\mathbf{b}_k(n) = [b_{k,1}(n), \dots, b_{k,m}(n), \dots, b_{k,M}(n)]^{\mathrm{T}}. \tag{3}$$

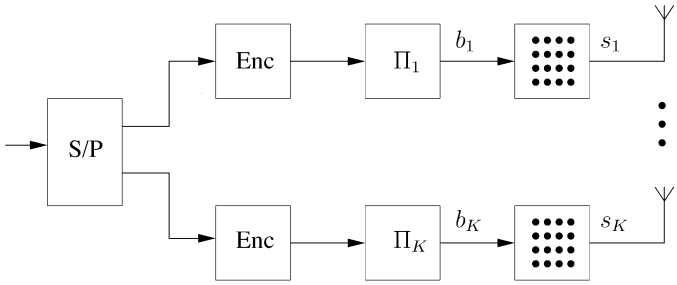

Fig. 1. BICM encoder (Enc) and modulator (Π_k: interleavers).

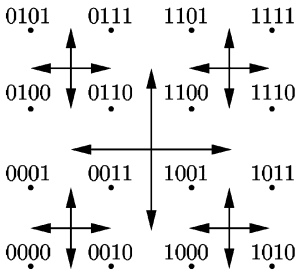

Fig. 2. BP 16-QAM mapping.

A symbol mapper performs nonlinear mapping $\mathbf{b}_k(n) \rightarrow s_k(n) \in S$ from the segments of bits in (3) into constellation points according to the selected mapping rule[1]. The symbol mapper is assumed to have normalized average energy so that $\mathrm{E}\{|s_k(n)|^2\} = 1$.

The mapped symbols of all transmit antennas are given as a length KN vector

$$\mathbf{s} = [\mathbf{s}^{\mathrm{T}}(1), \ldots, \mathbf{s}^{\mathrm{T}}(n), \ldots, \mathbf{s}^{\mathrm{T}}(N)]^{\mathrm{T}} \tag{4}$$

where

$$\mathbf{s}(n) = [s_1(n), \ldots, s_k(n), \ldots, s_K(n)]^{\mathrm{T}}. \tag{5}$$

C. MLBICM Coding and Modulation

The symbol mapping principle for the multilevel modulation is hierarchical block-partitioning (BP) with a square QAM constellation. The mapping uses identical bit-to-position allocation throughout all hierarchy levels, while in related mapping methods—studied, e.g., in [21] and [28]—the allocation changes between hierarchy levels. An illustration of the construction of a BP 16-QAM constellation is shown in Fig. 2. The minimum distance of the constellation points is different at each hierarchy level, resulting in unequal error protection characteristic when a single channel code is utilized commonly for all hierarchy levels.

The transmitted MLBICM symbols are constructed as illustrated in Fig. 3 in the following manner. The bits to be transmitter over the kth antenna are further demultiplexed into M parallel levels, which are channel encoded and interleaved in parallel with different random interleavers. The resulting M parallel sequences are segmented into groups of M bits so that each interleaved level defines a single bit in each group. In an identical manner to the BICM scheme, the segmented bits for each frame of length N can be expressed by the vectors (1)–(3), the only difference being the construction of the modulation through the use of parallel encoders and interleavers. We use the definitions (1)–(3) also for MLBICM for convenience.

The BP mapper can be seen as a linear combination of the M BPSK-modulated symbols, where the segment of encoded bits is multiplied with a complex weight vector $\mathbf{z}$ and summed up into QAM symbols. The weight vector consists of elements z_m, that are real for m being odd, and $z_m = iz_{m-1}$ for m being even. If the M-level linear BP mapper with its levels being ordered by decreasing amplitude is given as

$$\mathbf{z} = [z_1, \ldots, z_m, \ldots, z_M]^{\mathrm{T}} \tag{6}$$

constrained to $\mathbf{z}^{\mathrm{H}}\mathbf{z} = 1$, the mapped symbols within a frame are given as a vector

$$\underline{\mathbf{s}} = [\underline{\mathbf{s}}^{\mathrm{T}}(1), \ldots, \underline{\mathbf{s}}^{\mathrm{T}}(n), \ldots, \underline{\mathbf{s}}^{\mathrm{T}}(N)]^{\mathrm{T}} \tag{7}$$

where the transmitted symbols of the K antennas for time instant n are given by

$$\underline{\mathbf{s}}(n) = [\underline{s}_1(n), \ldots, \underline{s}_k(n), \ldots, \underline{s}_K(n)]^{\mathrm{T}} \tag{8}$$

and each symbol can be given as

$$\underline{s}_k(n) = \mathbf{z}^{\mathrm{T}}\mathbf{b}_k(n). \tag{9}$$

The symbol sequence for the whole frame can also be expressed as

$$\underline{\mathbf{s}} = (\mathbf{I}_N \otimes \mathbf{z})\mathbf{b} \tag{10}$$

$$= \mathbf{Z}\mathbf{b} \tag{11}$$

where $\otimes$ denotes the Kronecker product and $\mathbf{I_N}$ is an identity matrix of dimension N.

D. Received Signal

The system employs multiple antennas for receiving the composite signal. The space-time multipath channel matrix $\mathbf{H}$ with L separable multipaths, K transmitter, and J receive antennas is given as

$$\mathbf{H} = [\mathbf{H}(1), \ldots, \mathbf{H}(n), \ldots, \mathbf{H}(N)] \tag{12}$$

with

$$\mathbf{H}(n) = [\tilde{\mathbf{h}}_1(n), \ldots, \tilde{\mathbf{h}}_k(n), \ldots, \tilde{\mathbf{h}}_K(n)] \tag{13}$$

[1]For notational simplicity in describing multiple schemes, we consider the bits having one of the values $\{1, -1\}$.

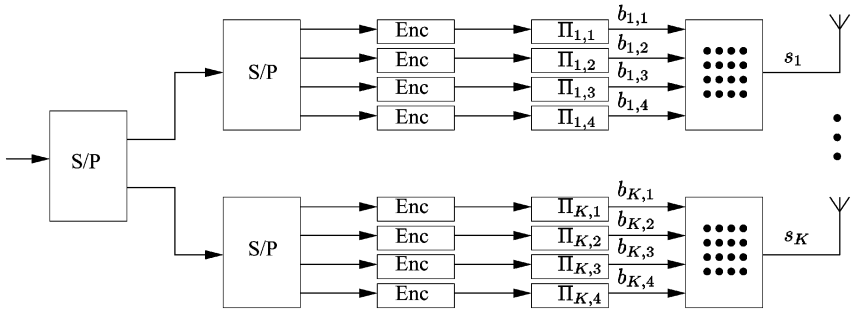

Fig. 3. MLBICM encoder (Enc) and modulator ($\Pi_{k,m}$: interleavers).

where $\tilde{\mathbf{h}}_k(n) = [\mathbf{0}^{\mathrm{T}}_{(n-1)J}, \mathbf{h}^{\mathrm{T}}_k(n), \mathbf{0}^{\mathrm{T}}_{(N-n+1)J}]^{\mathrm{T}}$ incorporates the channel response for the antenna k as

$$\mathbf{h}_k(n) = \left[\mathbf{h}^{\mathrm{T}}_{k,1}(n), \ldots, \mathbf{h}^{\mathrm{T}}_{k,l}(n), \ldots, \mathbf{h}^{\mathrm{T}}_{k,L}(n)\right]^{\mathrm{T}} \tag{14}$$

with

$$\mathbf{h}_{k,l}(n) = [h_{k,l,1}(n), \ldots, h_{k,l,j}(n), \ldots, h_{k,l,J}(n)]^{\mathrm{T}}. \tag{15}$$

The column vector $\mathbf{0}_q$ contains q zeros. As shown, we require that the the received power per antenna is normalized so that

$$\mathrm{E}\left\{\sum_{k=1}^{K}\sum_{l=1}^{L}|h_{k,l,j}|^2\right\} = 1. \tag{16}$$

When the BICM symbols (4) pass through the frequency selective channel the received signal, embedded in complex Gaussian noise $\mathbf{w}$ with power spectral density N_0 is given as

$$\mathbf{r} = \mathbf{H}\mathbf{s} + \mathbf{w}. \tag{17}$$

The corresponding received MLBICM signal with the transmitted symbols given by (7) can be expressed as

$$\underline{\mathbf{r}} = \mathbf{H}\underline{\mathbf{s}} + \mathbf{w} \tag{18}$$

$$= \mathbf{H}\mathbf{Z}\mathbf{b} + \mathbf{w}. \tag{19}$$

The representation in (19) allows us to consider the multilevel mapping as a part of the channel, simplifying the resulting receiver design.

III. Turbo Equalization of BICM

The turbo equalizer considered in this paper for BICM is the algorithm presented in [6] with extensions to a MIMO case. The equalizer structure consists of a soft-in-soft-out (SISO) equalizer block and SISO channel decoder blocks for each transmit antenna separated by interleaving and de-interleaving, as depicted in Fig. 4. The equalizer block performs soft interference cancellation using the channel decoder feedback. An MMSE filter is then defined for the filtering of the residual and for the computation of the extrinsic symbol likelihoods at the output of the equalizer block. The bit likelihoods are computed with a soft de-mapper that treats the equalizer output as the output of an equivalent Gaussian channel [2].

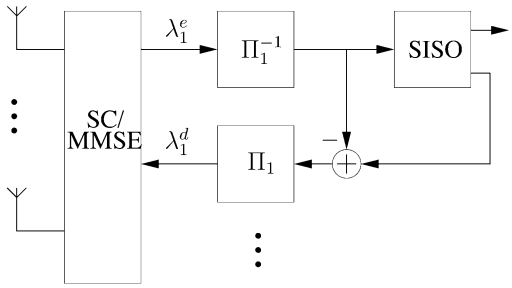

Fig. 4. BICM turbo equalizer.

The computations proceed as follows. The first two moments of the soft symbol estimates are obtained using channel decoder feedback for each k and n as

$$\hat{s}_k(n) = \mathrm{E}\{s_k(n)\} = \sum_{s_i \in S} s_i P_a(s_k(n) = s_i) \tag{20}$$

$$\mathrm{E}\{|\hat{s}_k(n)|^2\} = \sum_{s_i \in S} |s_i|^2 P_a(s_k(n) = s_i) \tag{21}$$

where P_a is the symbol *a priori* probability. Assuming the feedback consists of independent bit likelihoods, P_a can be computed as [2]

$$P_a(s_k(n) = s_i) = 2^{-M}\prod_{m=1}^{M}1 - 2b_{k,m}(n)\tanh\left(\frac{\lambda^d_{k,m}(n)}{2}\right) \tag{22}$$

where $\lambda^d_{k,m}(n)$ is the extrinsic likelihood ratio of bit $b_{k,m}(n)$ provided by the decoder. The *a priori* symbol mean given by (20) is then used to cancel signal components estimated with *a priori* information from the received signal to provide a residual as

$$\tilde{\mathbf{r}} = \mathbf{r} - \mathbf{H}\hat{\mathbf{s}} \tag{23}$$

where we have also canceled the desired signal component to be able to utilize the residual for all k. The MMSE minimization problem

$$\arg\min_{\mathbf{u}_k(n)} |s_k(n) - \mathbf{u}^{\mathrm{H}}_k(n)(\tilde{\mathbf{r}}(n) + \mathbf{h}_k(n)\hat{s}_k(n))|^2 \tag{24}$$

where $\tilde{\mathbf{r}}(n)$ consists of the $(n-1)J+1\ldots(N-n+1)J-1$th elements of $\mathbf{r}$, is then solved for each n and k to compute the filter taps $\mathbf{u}_k(n)$. The filter input in (24) consists of the desired signal component added to the residual (23). If the feedback $\hat{\mathbf{s}}$ is adequately randomized by interleaving, it can be assumed uncorrelated, in which case its covariance matrix becomes diagonal

$$\mathbf{\Lambda} = \mathrm{diag}\{\mathrm{E}\{|\mathbf{s}(n)|^2\} - |\hat{\mathbf{s}}(n)|^2\} \tag{25}$$

with which the covariance matrix of the residual in (23) becomes

$$\mathbf{\Sigma} = \mathbf{H}\mathbf{\Lambda}\mathbf{H}^{\mathrm{H}} + \sigma_0^2\mathbf{I} \tag{26}$$

where $\sigma_0^2 = N_0MJ/K$ is the noise variance. With (26), we can formulate the filter coefficients for symbol n as

$$\mathbf{u}_k^{\mathrm{H}}(n) = \mathbf{h}_k^{\mathrm{H}}(n)\mathbf{\Sigma}^{-1}(n) \tag{27}$$

where $\mathbf{\Sigma}(n)$ contains the $(n-1)J+1\ldots(n+L-1)J$th rows and $(n-1)J+1\ldots(n+L-1)J$th columns of $\mathbf{\Sigma}$. After decomposing the filter output to the desired component and the residual, and invoking the matrix inversion lemma, the following two intermediate variables are computed as

$$\alpha_k(n) = \mathbf{u}_k^{\mathrm{H}}(n)\mathbf{h}_k(n) \tag{28}$$

$$\beta_k(n) = \frac{1}{1+\alpha_k(n)|\hat{s}_k(n)|^2} \tag{29}$$

to be utilized in the computation of the filter output as

$$x_k(n) = \beta_k(n)(\alpha_k(n)\hat{s}_k(n) + \mathbf{u}_k^{\mathrm{H}}(n)\tilde{\mathbf{r}}(n)). \tag{30}$$

Notice that in (27) the covariance matrix inverse is common to and can be re-used for all k, and that the difference between filters of transmit antennas is due to the transmit antenna-wise channel responses. If the equalizer output (30) is seen as the output of an equivalent AWGN channel having $s_k(n)$ as input, the equivalent channel variance can be computed as

$$\nu_k(n) = \alpha_k(n)\beta_k(n)(1-\alpha_k(n)\beta_k(n)). \tag{31}$$

Since the elements of the diagonal matrix $\mathbf{\Lambda}(n)$ are not constant the MMSE solution is time-variant and (27)–(31) have to be computed for each n. The extrinsic bit log-likelihood is computed by using *a priori* information as [29]

$$\lambda_{k,m}^e(n) = \ln\frac{\sum_{s_i\in S_{\underline{\ }1}^m} P(s^m=s_i)e^{L_e(s_i)}}{\sum_{s_i\in S_1^m} P(s^m=s_i)e^{L_e(s_i)}} \tag{32}$$

where S_1^m and $S_{\underline{\ }1}^m$ define the subsets of S where the bit b_m takes the values 1 and -1, correspondingly, and $L_e(s_i)$ is the *a priori* likelihood of symbol point s_i based on information of all data bits within the segment other than m. The probability of each mapping point s_i in (32) is computed with the equalizer output as

$$P(s_k(n)=s_i) = \frac{1}{\nu_k(n)\pi}e^{-\frac{|x_k(n)-\alpha_k(n)\beta_k(n)s_i|^2}{\nu_k(n)}} \tag{33}$$

which approximates the equalizer output as Gaussian distributed with mean $\mu_k(n)$ and variance $\nu_k(n)$. After the equalization of each frame, deinterleaving, and SISO channel decoding are performed, and extrinsic information of both encoded transmitted bits and information bits is computed. The former is then fed back to the equalizer through the interleaver and utilized in another equalization iteration in the computation of (20)–(21) and (32). During the first iteration, when no *a priori* information of the transmitted bits is available, the equalizer reduces to a linear MMSE equalizer.

IV. Turbo Equalization of MLBICM

The equalizer algorithm described in Section III can be directly utilized in the detection of MLBICM. However, if the hierarchical structure of the mapping is exploited, a new equalizer structure with lower complexity can be derived. This section presents the derivation of the algorithm. As indicated by (19) the block-partitioned symbol constellation is treated as a linear combination of binary subconstellations, where each coding level of the multilevel encoder is utilized as the input to one binary (BPSK) subconstellation. The linear mapping is considered to be a part of the channel, as suggested by (17), excited by BPSK modulated symbols. A turbo equalizer is then defined, where most of the processing for equalization and decoding of each subconstellation can be performed in parallel [17]. The MMSE filter computation in the algorithm considers a single level as the desired signal. A block diagram of the equalizer and decoder (for one transmit antenna) is depicted in Fig. 5.

Equalization and decoding of levels is ordered. Code levels with largest weight z_m are decoded first, levels with the second largest weight from the second iteration onwards, and so on. For a 16-QAM square constellation, levels 1–2 (having equal weights) are equalized and decoded in the first iteration, and all levels 1–4 equalized and decoded on the second iteration onwards.

The equalizer algorithm is illustrated in more detail with a block diagram in Fig. 6. The figure also indicates which computation results can be reused for all detected bits, which are specific to one transmit antenna, and which are computed for each coding level. One common filter is used in the computation of the equalizer output of all subconstellations during one turbo iteration. The algorithm to obtain the estimate of the transmitted signal of one level is obtained by applying the algorithm in Section III for BPSK modulation. First, corresponding to (20), the expected value of the soft symbol estimates is computed as

$$\hat{b}_{k,m}(n) = \tanh\left(\underline{\lambda}_{k,m}^d(n)\Big/2\right) \tag{34}$$

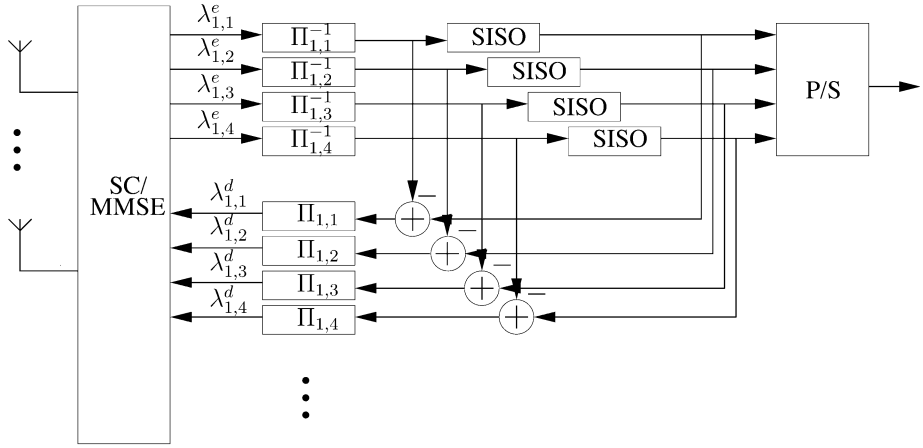

Fig. 5. MLBICM turbo equalizer.

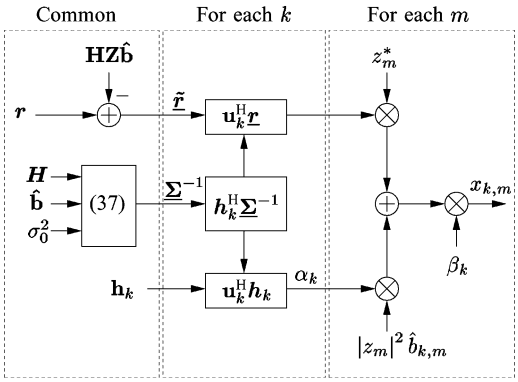

Fig. 6. MLBICM turbo equalizer block diagram, dotted line encloses postprocessing for one transmitter antenna k.

where $\underline{\lambda}_{k,m}^{d}(n)$ is the log-likelihood ratio provided by the kth user's decoder for bit $b_{k,m}(n)$. The residual is then computed as

$$\underline{\tilde{\mathbf{r}}} = \mathbf{r} - \mathbf{HZ}\hat{\mathbf{b}}. \tag{35}$$

The covariance matrix of the soft symbol estimates is then obtained similarly to (25) as

$$\underline{\boldsymbol{\Lambda}} = \mathrm{diag}\left\{1 - \left|\underline{\hat{b}}_{k,m}(n)\right|^2\right\} \tag{36}$$

to form the residual covariance matrix as

$$\underline{\boldsymbol{\Sigma}} = \mathbf{HZ}\underline{\boldsymbol{\Lambda}}\mathbf{Z}^{\mathrm{H}}\mathbf{H}^{\mathrm{H}} + \sigma_0^2\mathbf{I}. \tag{37}$$

Both the computation results of the residual in (35) and the covariance matrix in (37) are common to all k and m. For lower complexity, a banded version of the covariance matrix (37) is computed. Next, the filtering (27) and (28) are modified to take advantage of the linear model for the multilevel coded signal. The common filter for all levels of antenna k is given by

$$\underline{\mathbf{u}}_k^{\mathrm{H}}(n) = \mathbf{h}_k^{\mathrm{H}}(n)\underline{\boldsymbol{\Sigma}}^{-1}(n) \tag{38}$$

which is utilized in the computation of the intermediate variables as

$$\begin{aligned}\underline{\alpha}_k(n) &= \underline{\mathbf{u}}_k^{\mathrm{H}}(n)\mathbf{h}_k(n)\\ &= \mathbf{h}_k^{\mathrm{H}}(n)\underline{\boldsymbol{\Sigma}}^{-1}(n)\mathbf{h}_k(n)\end{aligned} \tag{39}$$

$$\underline{\beta}_{k,m}(n) = \frac{1}{1 + |z_m|^2\underline{\alpha}_k(n)|\hat{b}_{k,m}(n)|^2} \tag{40}$$

only the second of which is computed for each level. Finally, the prior soft symbol estimate of the level m is utilized in the filter output computation for level m as

$$\underline{x}_{k,m}(n) = \underline{\beta}_{k,m}(n)(|z_m|^2\underline{\alpha}_k(n)\hat{b}_{k,m}(n) + z_m^*\underline{\mathbf{u}}_k^{\mathrm{H}}(n)\underline{\tilde{\mathbf{r}}}(n)). \tag{41}$$

The M parallel channel decoders are then provided with the binary likelihood information computed as

$$\underline{\lambda}_{k,m}^{e}(n) = 4\frac{\Re\{\underline{x}_{k,m}(n)\}}{1 - |z_m|^2\underline{\alpha}_k(n)\underline{\beta}_{k,m}(n)}. \tag{42}$$

Note that (42) is the result of expressing (33) for BPSK modulation in logarithm domain. The parallel channel decoders operate independently without the need to exchange information as in multistage decoding [10]. Instead, *a priori* information exchange is carried out through the equalizer in the process of soft interference cancellation.

V. Channel Model-Based Comparison

One of the goals of the proposed MLBICM scheme is to utilize multilevel coding to enhance the convergence properties of the corresponding turbo equalizer. Up to now, however, convergence analysis of turbo equalizers has relied on simulation-based EXIT charts [30], [6], which restrict the analysis to fixed channels. Furthermore, EXIT analysis is valid for very long frame lengths, whereas we are mostly interested

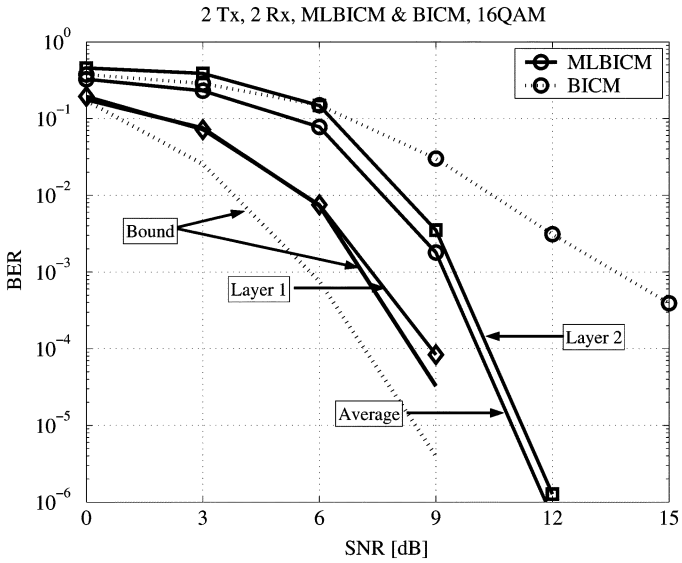

Fig. 7. BER of 16-QAM MLBICM and BICM.

in relatively short frames. As a result, we will resort to performance simulations in evaluating the proposed scheme in a fading channel. The MLBICM scheme with 16-QAM symbol constellation is compared to the standard Gray-mapped 16-QAM BICM with the corresponding receivers presented in Sections III and IV. The channel is assumed to be a five-path Rayleigh-fading channel with an average path energy having a decay factor of -2 dB between the consecutive paths. The paths were assumed to be mutually uncorrelated and fixed over a received frame, but varying frame-to-frame. Two transmit and receive antennas, and a fully spatially uncorrelated channel were assumed. Perfect channel knowledge was assumed at the receiver. The rate-$1/2$ convolutional code with generator polynomials (5, 7), a random interleaver, and a 512 information bit frame length were used for the both schemes. The frame length results in interleaver lengths of 1024 encoded bits for the BICM scheme and 256 encoded bits for each level in the MLBICM scheme. The log-MAP algorithm was utilized for the SISO decoding of the convolutional code. For the both schemes, the receivers perform six iterations of equalization and decoding.

The bit-error rates (BER) after the last iteration are presented in Fig. 7 as a function of average received SNR per receive antenna. Due to the unequal error protection (UEP) capability of the MLBICM, the performance is reported by multiple performance curves. Since each in-phase and quadrature pair of levels provide the same level of error protection, each of such pairs is referred to as one "layer." In the sequel, Layer-1 incorporating the levels 1 and 2 determines the constellation quadrant, and Layer-2 incorporating levels 3 and 4 determines the point within the quadrant. It is found that the average BER over both layers of the MLBICM transmission is dominated by errors at Layer-2, which is logical considering the difference in minimum distance between layers and the use of identical channel codes for all levels.

To illustrate the performance bounds, the schemes were simulated assuming perfect feedback. The resulting average BER's are reported in Fig. 7, indicating that the BICM bound is better than the MLBICM bound. The BICM scheme performance, however, remains far from the bound, whereas the MLBICM scheme performance is only 2 dB off the bound within the BER range of $10^{-2} \ldots 10^{-4}$. The results implicitly illustrate the convergence properties of the turbo equalizers for the two transmission schemes in the selected channel conditions.

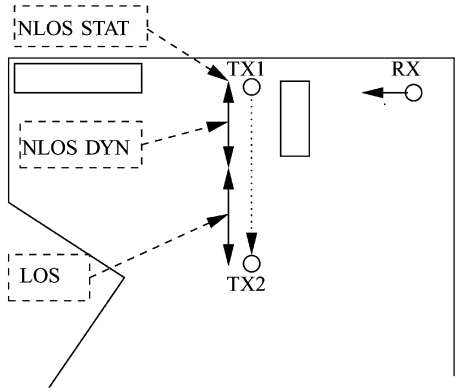

Fig. 8. Measurement scenario: transmitter's static/dynamic NLOS and LOS regions on route from TX1 to TX2.

We notice BICM performs poorly compared to MLBICM in the simulated channel. In general, overall performances of turbo-equalization systems are largely related to the convergence properties of the systems, which are affected by the channel code, mapping rule and channel realization. The mappings of both MLBICM and BICM divide bits into reliability classes [31], but in BICM they are encoded with a single channel code, as opposed to MLBICM where the classes are separated into different levels. Thus, from the decoding perspective, MLBICM Layer-2 bits do not contribute to the reliability of Layer-1 bits. On the other hand, due to the separation of the layers, MLBICM can utilize the reliable feedback from Layer-1 in equalization, which can justify the rapid improvement of Layer-2 performance at high signal-to-noise ratio (SNR).

The discussion above does not account for the impact of the channel properties to the differences in performance between MLBICM and BICM. For a more complete comparison, we must study how the performance is related to the variation of channel's spatio-temporal conditions, preferably in realistic propagation conditions. If we wish to have a realistic view of the performance difference between the two schemes, the channel model to be used has to be accurate enough to express the MIMO broadband channel. Unfortunately, few accurate and widely accepted models exist for such channels. As illustrated below, one possibility for realistic evaluations is through the use of channel measurement data.

VI. MIMO Measurements for Realistic Performance Evaluation

A. Measurement Scenario and Propagation Characterization

A series of measurements took place within a large courtyard at the campus of the Ilmenau University of Technology, a sketch of which is given in Fig. 8. The place is completely surrounded by a building of about 15 m height, and several different metal

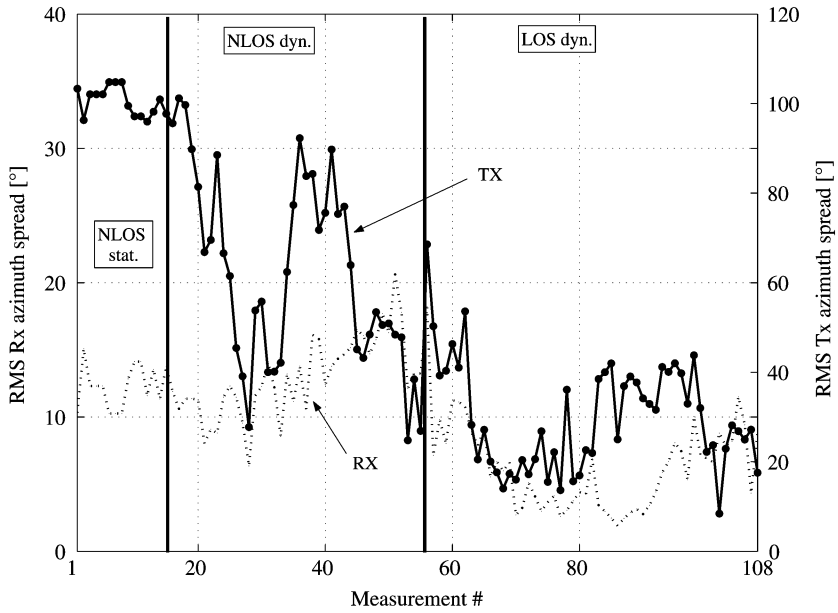

Fig. 9. Channel azimuth spread: solid line TX, dotted line RX.

objects (containers, mesh fence, and tubes) were located within the courtyard. Fig. 8 shows the selected measurement track that covers a non line-of-sight (NLOS) part of approximately 3 m from the position TX1, where the line-of-sight (LOS) was obstructed by a high metal container, and a LOS part for the rest of the track. The transmit antenna, an omnidirectional 16-element uniform circular array (UCA), mounted at a height of 2.10 m, was first held in-place at TX1 and then moved at walking speed toward the position TX2. For the receive antenna, an eight-element uniform linear array (ULA), mounted at a height of 1.67 m, was used. All measurements were conducted at 5.2 GHz carrier frequency with a channel sounding system bandwidth of 120 MHz. The measured channel impulse responses (CIR) were normalized to have unity mean energy over all transmit and receive antenna pairs. The normalization results in a stable average received power, whereas short-term fading effects are preserved. Two transmit and two receive antennas were selected from the measurement equipment and the 108 snapshots of the corresponding channel impulse response data was used in the simulations. The approximate minimum element spacings were two wavelengths at the transmitter and four wavelengths at the receiver side.

Using a superresolution path parameter estimation technique [22], three significantly different propagation conditions, static NLOS, dynamic NLOS, and LOS, can be identified. A detailed insight into the spatio-temporal multipath structure of the measurement area can be found in [9]. Fig. 9 highlights the propagation conditions in terms of rms transmitter and receiver azimuthal spreads. The largest rms azimuthal spread at the transmitter side can be found within the first 15 snapshots, where the transmitter was not moving. This indicates a multipath-rich environment in the NLOS propagation section. The fluctuation in the spreads is due to minor environmental changes. During the measurement of snapshots between 16 and 55 the transmitter was moving along the measurement track from position TX1 to approximately the middle of the track. During this section the propagation is still NLOS, but exhibiting medium transmitter and receiver azimuthal spreads. For the rest of the track the propagation is LOS and the azimuthal spreads are significantly lower compared to the NLOS sections. Receive side azimuthal spread is much smaller than the transmit side due to the 120° beamwidth of the ULA elements used. These three different propagation characteristics (NLOS static, NLOS dynamic and LOS dynamic) are considered in the following performance evaluations and show significantly different performance figures between the MLBICM and BICM systems.

B. Measurement Data-Based Performance Results

In measurement data-based simulations, the transmitted signal was convolved with the transmitter filter, the measured CIR, and the receiver filter, whereby the two filters define the system bandwidth. Results of performance evaluations for a class of turbo-equalizers in measured MIMO channels are presented [26], [9]. Our motivation is to study the throughput efficiency offered by the MLBICM scheme and to compare it with that of the standard BICM scheme. The results will enable us to evaluate the characteristics of the link as seen by the higher protocol layers when the channel conditions vary. We evaluate the frame-error rate (FER) of the two schemes in a measured channel using a two transmit—two receive antenna configuration to examine the throughput efficiency (TPeff) ([32, ch. 15]) given by

$$\mathrm{TPeff} = R(1 - \mathrm{FER}) \tag{43}$$

where selective-repeat ARQ with infinite buffering is assumed, with R being the channel code rate. The transmitter and receiver employ root-raised cosine filters, both with a roll-off factor of 0.25, so that the simulated channel bandwidth of 25 MHz translates into a symbol rate of 20 Msym/s. The overall maximum throughput efficiency of 0.5 then corresponds to a data rate of 80

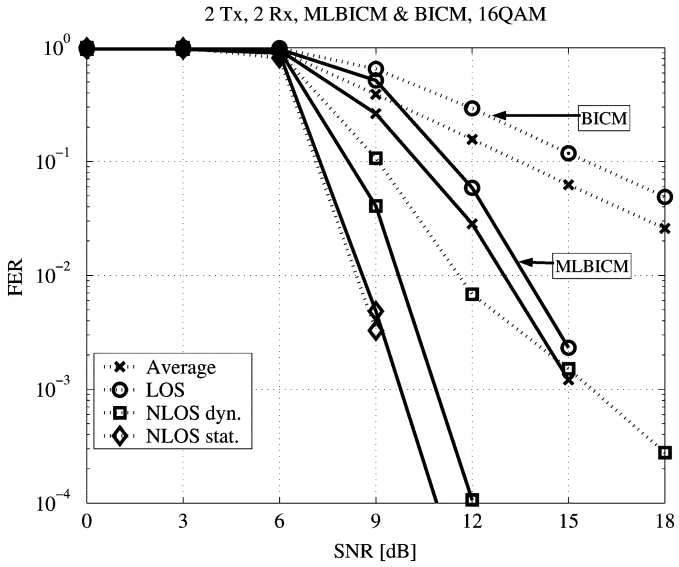

Fig. 10. MLBICM average FER over levels (solid line) and BICM FER (dotted line) on static NLOS, dynamic NLOS and LOS regions.

Mbits/s in the tested two-by-two configuration using 16-QAM and rate one-half channel coding with 4 bits/symbol total spectral efficiency. One hundred eight snapshots from the measurement track were used, and 350 frames were transmitted per snapshot. Other system parameters were identical to those described in Section V.

Fig. 10 reports the average FER over code levels for MLBICM and the average FER of BICM, and indicates a generic trend in the performance of the studied schemes. Both MLBICM and BICM achieve excellent performances in the static NLOS multipath rich environment, with BICM performing somewhat better. The difference between the schemes can be found in channels with less multipath richness. In those scenarios (dynamic NLOS, LOS) the both schemes degrade in performance compared to the static NLOS case, but the MLBICM system performance loss is more graceful than that of the BICM system. The LOS channel condition dominates the results for the both schemes when the average FER over all scenarios is considered. It should be noted the average FER for MLBICM is computed after re-multiplexing the decoded streams, and for which errors from Layer-2 dominate the result. In general, the result indicates that MLBICM with turbo-equalization is less sensitive to the variation in channel conditions than the BICM counterpart. It indicates that the MLBICM scheme exhibits a minor loss compared to the BICM scheme in the best channel conditions of the static NLOS scenario, but offers significant gain in other scenarios identified. Layer-1 of the MLBICM has higher error protection than Layer-2 and is able to provide reliable feedback to the equalizer in a large variation of channel conditions. Thus, the MLBICM turbo-equalizer can reach partial convergence even though all coding levels cannot be successfully decoded. The convergence of the BICM scheme, on the other hand, depends on reliable decoding and feedback of all the transmitted information bits.

The average TPeff over the measurement track shown in Fig. 11 indicates the same tendency: The BICM scheme offers a small advantage in the static NLOS channel when $\mathrm{TPeff} < 0.1$, but in all other cases MLBICM offers superior performance, especially when TPeff approaches its maximum $(=0.5)$.

In the results reported in Fig. 11, it is assumed that a single ARQ controller process handles the retransmission and the whole 512-bit frame is retransmitted in case of frame errors. This approach is denoted by S-ARQ in the sequel to indicate the single ARQ controller. The total retransmission probability and the resulting TPeff of MLBICM is dominated by errors from Layer-2. If the two layers are handled by separate ARQ controllers, this can be avoided and thereby the overall TPeff can be improved. Fig. 12 shows the average TPeff for MLBICM over the measurement track with layered ARQ (L-ARQ), where each of the two ARQ controllers handle retransmissions on a single layer. The maximum throughput efficiency of each layer is scaled to match the spectral efficiency of one layer when computing the TPeff of (43). Fig. 12 shows the difference in TPeff between the two layers and demonstrates that the total TPeff is the TPeff sum over the layers. For further analysis of the gain in different channel scenarios, we compare the TPeffs with S-ARQ MLBICM, L-ARQ, MLBICM, and the standard BICM scheme in the two extreme channel conditions: static NLOS and LOS.

Fig. 13 shows the TPeffs with S-ARQ and L-ARQ MLBICM averaged over the measurement snapshots in static NLOS channel conditions. For comparison, the TPeff with the BICM scheme in the same conditions is shown. The average TPeff with BICM is better than that with MLBICM and S-ARQ, as already indicated in Fig. 11. However, since the total average TPeff of MLBICM with L-ARQ is equal to the mean of the average TPeff in the two layers, the MLBICM scheme with L-ARQ offers superior performance to both MLBICM and BICM schemes utilizing S-ARQ. It should be recognized that the comparison is not completely fair due to the larger frame length of BICM, which slightly inflates the mean FER. Shortening the frame length with BICM is problematic, however, due to convergence problems with short interleaving. Fig. 13 demonstrates how L-ARQ provides a smooth transition from low to high TPeff as the SNR is improved.

The performance of L-ARQ MLBICM and BICM is emphasized in the LOS channel conditions, where the MLBICM's FER performance is better than that of BICM. Fig. 14 shows the LOS results showing a superior TPeff of MLBICM with the both types of ARQ. A gain of 2 dB with L-ARQ MLBICM can be seen at $\mathrm{TPeff} > 0.2$.

VII. Discussion

The main drawback of the proposed L-ARQ scheme is the requirement for multiple parallel ARQ processes. A small overhead is also brought by the utilization of separate error detection codes for each ARQ process. For practical implementations a further consideration in the detailed design of the L-ARQ scheme must be given to the required buffer length. Distinctly and consistently different retransmission probabilities of the layers will require different buffer sizes for the ARQ processes. The total buffer requirement is likely

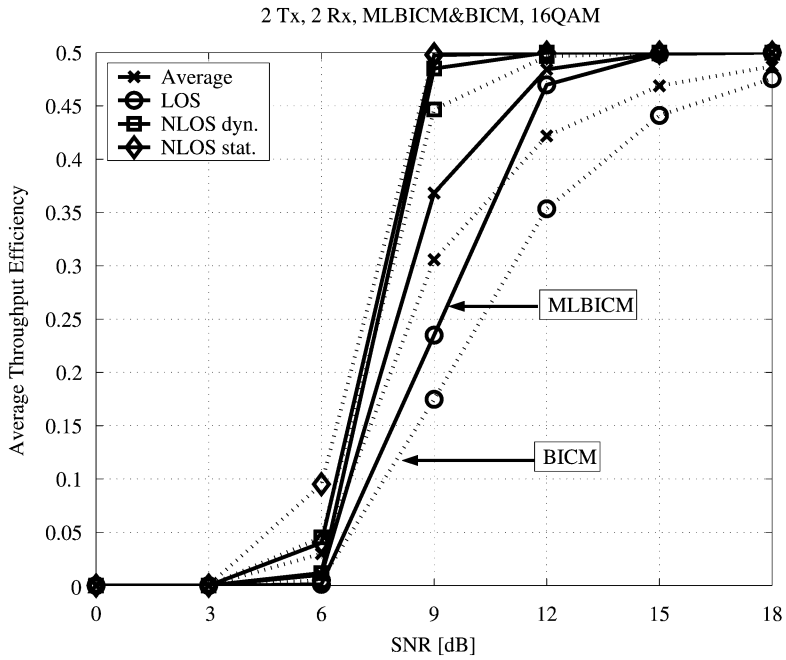

Fig. 11. Average throughput efficiency of MLBICM (solid line) and BICM (dotted line) on static NLOS, dynamic NLOS and LOS regions.

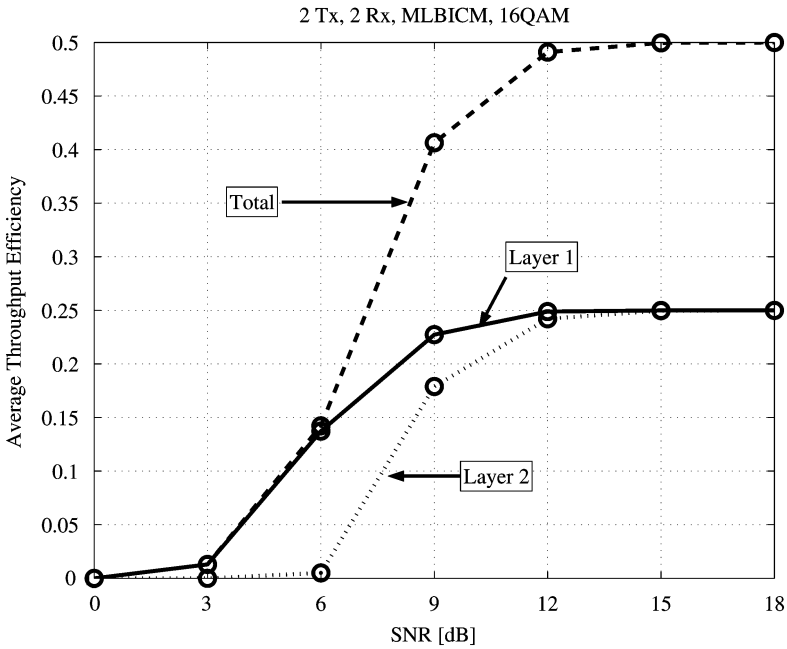

Fig. 12. Average throughput efficiency of MLBICM over the measurement track when layers have separate ARQ (L-ARQ).

to be lower for L-ARQ than for S-ARQ due to the smaller size of retransmissions.

An alternative to utilizing L-ARQ would be to design the channel code according to the known design rules for multilevel coding [21] so that all levels perform at a target operation point. A low-complexity scheme could utilize component codes punctured to different rates according to the properties of the modulation and maintain the convenience of using a single encoder and a single decoder. Whether such a design would maintain the robust convergence properties of the scheme proposed in this paper, which depend on the reliable decoding of Layer-1 bits throughout a wide range of SNR's and channel conditions, remains a topic of further study.

VIII. Summary

An efficient scheme for packet-based data transmission using broadband single-carrier signaling was proposed. The proposed scheme allows for efficient MIMO turbo-equalization at the receiver to be performed, and provides data throughput robustness in varying spatio-temporal channel characteristics. Performance evaluation results were obtained through simulations in

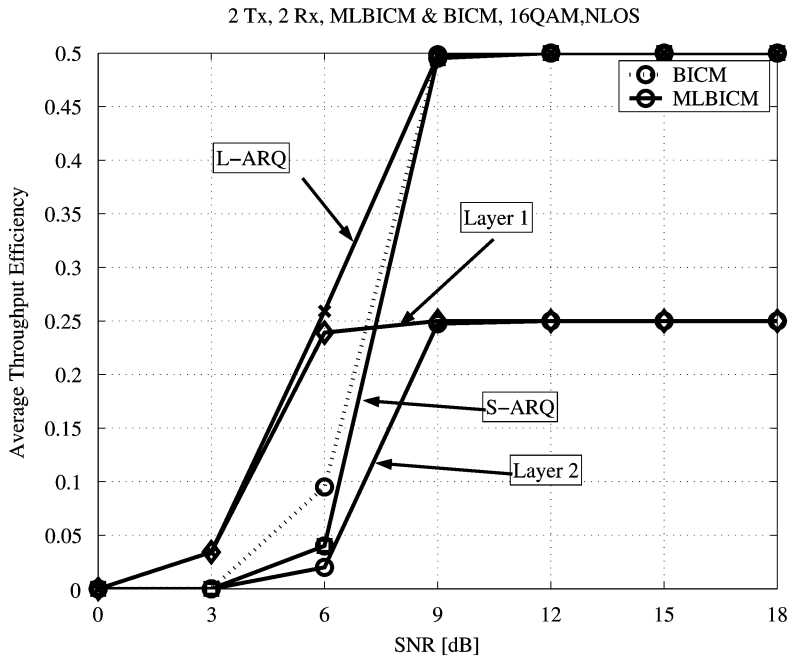

Fig. 13. Average throughput efficiency of MLBICM (solid line) and BICM (dotted line) in static NLOS, MLBICM reported both with S-ARQ and L-ARQ.

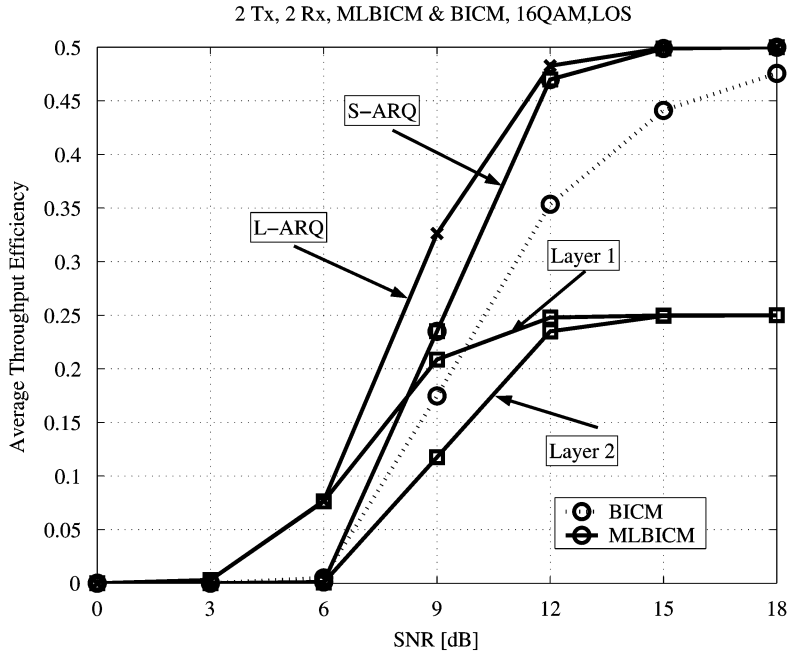

Fig. 14. Average throughput efficiency of MLBICM (solid line) and BICM (dotted line) and in LOS, MLBICM reported both with S-ARQ and L-ARQ.

measured channel conditions, and evaluated with the assistance of spatial channel parameter estimation using a superresolution technique. The proposed scheme was shown to at least match and in many cases exceed the throughput efficiency of BICM in the tested channel conditions. It has been shown that when the unequal error protection of the modulation is taken into account in the ARQ algorithm design by separating the ARQ processes of the differently protected levels, further performance improvement can be achieved.

ACKNOWLEDGMENT

The authors wish to thank MEDAV GmbH for their support in providing us with field measurement data obtained using the RUSK MIMO channel sounder. We also thank the colleagues at the Ilmenau University of Technology for conducting the measurements and data analysis. Finally, the anonymous reviewers are thanked for their helpful comments which helped improve the paper.

REFERENCES

[1] C. Douillard, C. M. Jezequel, C. Berrou, A. Picart, P. Didier, and A. Glavieux, "Iterative correction of intersymbol interference: Turbo-equalization," *Eur. Trans. Telecommun.*, vol. 6, no. 5, pp. 507–511, Sep. 1995.

[2] X. Wang and H. V. Poor, "Iterative (turbo) soft interference cancellation and decoding for coded CDMA," *IEEE Trans. Commun.*, vol. 47, no. 7, pp. 1046–1061, Jul. 1999.

[3] D. Reynolds and X. Wang, "Low-complexity turbo-equalization for diversity channels," in *Signal Processing*: Elsevier Science Publishers, May 2000, vol. 81, pp. 989–995.

[4] M. Tüchler, A. C. Singer, and R. Koetter, "Minimum mean squared error equalization using a priori information," *IEEE Trans. Signal Processing*, vol. 50, no. 3, pp. 673–683, Mar. 2002.

[5] G. Caire, G. Taricco, and E. Biglieri, "Bit-interleaved coded modulation," *IEEE Trans. Inform. Theory*, vol. 44, pp. 927–946, May 1998.

[6] A. Dejonghe and L. Vandendorpe, "Turbo-equalization for multilevel modulation: An efficient low-complexity scheme," in *Proc. IEEE Int. Conf. Commun.*, vol. 3, New York, Apr. 28–May 2 2002, pp. 1863–1867.

[7] S. L. Ariyavisitakul, "Turbo space-time processing to improve wireless channel capacity," *IEEE Trans. Commun.*, vol. 48, no. 8, pp. 1347–1359, Aug. 2000.

[8] T. Abe and T. Matsumoto, "Space-time turbo equalization in frequency-selective MIMO channels," *IEEE Trans. Veh. Technol.*, vol. 52, no. 3, pp. 469–475, May 2003.

[9] C. Schneider, U. Trautwein, T. Matsumoto, and R. Thomä, "Dependency of turbo MIMO equalizer performances on spatial and temporal multipath channel structure—A measurement based evaluation," in *Proc. IEEE Veh. Technol. Conf.*, vol. 1, Jeju, Korea, Apr. 22–25, 2003.

[10] H. Imai and S. Hirakawa, "A new multilevel coding method using error correcting codes," *IEEE Trans. Inform. Theory*, vol. 23, no. 3, pp. 371–377, May 1977.

[11] M. Isaka and H. Imai, "Hierarchical coding based on adaptive multilevel bit-interleaved channels," in *Proc. IEEE Veh. Technol. Conf.*, vol. 3, Tokyo, Japan, May 15–18, 2000, pp. 2227–2231.

[12] T. M. Cover and J. A. Thomas, *Elements of Information Theory*. New York: Wiley, 1991.

[13] R. Morelos-Zaragoza, M. Fossorier, S. Lin, and H. Imai, "Multilevel coded modulation for unequal error protection and multistage decoding—Part I: Symmetric constellations," *IEEE Trans. Commun.*, vol. 48, no. 2, pp. 204–213, Feb. 2000.

[14] M. Isaka, M. Fossorier, R. Morelos-Zaragoza, S. Lin, and H. Imai, "Multilevel coded modulation for unequal error protection and multistage decoding—Part II: Asymmetric constellations," *IEEE Trans. Commun.*, vol. 48, no. 5, pp. 774–786, May 2000.

[15] T. Woerz and J. Hagenauer, "Iterative decoding for multilevel codes using reliability information," in *Proc. IEEE Global Telecommun. Conf.*, vol. 3, Orlando, FL, Dec. 1992, pp. 1779–1784.

[16] M. Isaka and H. Imai, "On the iterative decoding of multilevel codes," *IEEE J. Sel. Areas Commun.*, vol. 19, no. 5, pp. 935–943, May 2001.

[17] K. Kansanen and T. Matsumoto, "Turbo equalization of multilevel coded QAM," in *Proc. IEEE Work. Signal Proc. Adv. Wireless Commun.*, Rome, Italy, Jun. 15–18, 2003.

[18] K. Holdsworth, D. Taylor, and R. Pullman, "On combined equalization and decoding of multilevel coded modulation," *IEEE Trans. Commun.*, vol. 49, no. 6, pp. 943–947, Jun. 2001.

[19] N. D. Doan and R. Rajatheva, "Turbo equalization for nonbinary coded modulation schemes over frequency-selective fading channels," in *Proc. IEEE Veh. Technol. Conf.*, vol. 3, Tokyo, Japan, May 15–18, 2000, pp. 2217–2221.

[20] ——, "Bit-interleaved coded modulation with iterative decoding and 8PSK signaling," *IEEE Trans. Commun.*, vol. 50, no. 8, pp. 1250–1257, Aug. 2002.

[21] U. Wachsmann, R. Fischer, and J. Huber, "Multilevel codes: Theoretical concepts and practical design rules," *IEEE Trans. Inform. Theory*, vol. 45, no. 5, pp. 1361–1391, Jul. 1999.

[22] R. Thomä, D. Hampicke, A. Richter, G. Sommerkorn, and U. Trautwein, "MIMO measurement for double-directional channel modeling," *Euro. Trans. Telecommun.*, vol. 12, no. 5, pp. 427–438, Sep. 2001.

[23] A. Richter, M. Landmann, and R. Thomä, "Maximum likelihood channel parameter estimation from multidimensional channel sounding measurements," in *Proc. IEEE Veh. Technol. Conf.*, vol. 2, Jeju, Korea, Apr. 22–25, 2003, pp. 1056–1060.

[24] M. Haardt, R. Thomä, and A. Richter, "Multidimensional high-resolution parameter estimation with applications to channel sounding," in *High-Resolution and Robust Signal Processing*, Y. Hua, A. Gershman, and Q. Cheng, Eds. New York: Marcel Dekker, 2003, pp. 253–337.

[25] B. H. Fleury, M. Tschudin, R. Heddergott, D. Dahlhaus, and K. I. Pedersen, "Channel parameter estimation in mobile radio environments using the SAGE algorithm," *IEEE J. Sel. Areas Commun.: Wireless Commun. Series*, vol. 17, no. 3, pp. 434–450, Mar. 1999.

[26] U. Trautwein, T. Matsumoto, C. Schneider, and R. Thomä, "Exploring the performance of turbo MIMO equalizer in real field schnarios," in *Proc. Int. Symp. Wireless Pers. Multimedia Commun.*, vol. 1, Honolulu, HI, Oct. 2002.

[27] G. Foschini, "Layered space-time architecture for wireless communication in a fading environment when using multi-element antennas," *Bell Labs Tech. J.*, vol. 1, no. 2, pp. 41–59, Aug. 1996.

[28] P. K. Vitthaladevuni and M.-S. Alouini, "A recursive algorihtm for the exact BER computation of generalized hierarchical QAM constellations," *IEEE Trans. Inform. Theory*, vol. 49, no. 1, pp. 297–307, Jan. 2003.

[29] S. ten Brink, "Iterative demapping and decoding for multilevel modulation," in *Proc. IEEE Global Telecommun. Conf.*, vol. 1, Sydney, NSW, Australia, Nov. 8–12, 1998, pp. 579–584.

[30] M. Tüchler, R. Koetter, and A. C. Singer, "Turbo equalization: Principles and new results," *IEEE Trans. Commun.*, vol. 50, no. 5, pp. 754–767, May 2002.

[31] P.-M. Fortune, L. Hanzo, and R. Steele, "On the computation of 16-QAM and 64-QAM performance in rayleigh-fading channels," *IEICE Trans. Commun.*, vol. E75-B, no. 6, pp. 466–475, Jun. 1992.

[32] S. Lin and D. Costello, *Error Control Coding*. Englewood Cliffs, NJ: Prentice-Hall, 1983.

Kimmo Kansanen (S'99–M'05) received the M.Sc. degree from the University of Oulu, Oulu, Finland, in 1998. Since 1999, he has pursued the Doctoral degree at the Centre for Wireless Communication, University of Oulu.

His research interests include joint detection in fading channels, iterative equalization and multiuser detection, and communication theory.

Christian Schneider received the Diploma degree in electrical engineering from the Technische Universität Ilmenau, Ilmenau, Germany, in 2001. He is currently pursuing the Dr.-Ing. degree with the Electronic Measurement Research Lab, Institute of Communications and Measurement Engineering, Technische Universität Ilmenau.

His research interests include space-time signal processing, turbo techniques, multidimensional channel sounding, channel characterization, and channel Madelina.

Tad Matsumoto (M'84–SM'95) received the B.S., M.S., and Ph.D. degrees in electrical engineering from Keio University, Yokohama-shi, Japan, in 1978, 1980, and 1991, respectively.

He joined Nippon Telegraph and Telephone Corporation (NTT) Japan, in April 1980. From April 1980 to January 1991, he researched signal transmission techniques such as modulation/demodulation, error control, and radio link design schemes for first- and second-generation mobile communications systems. In July 1992, he transferred to NTT DoCoMo, where he researched code division multiple access (CDMA) techniques. From 1992 to 1994, he served as a part-time lecturer with Keio University, Japan. In April 1994, he transferred to NTT America, where he served as a Senior Technical Advisor with the NTT-NEXTEL Communications joint project. In March 1996, he returned to NTT DoCoMo, and he was appointed Head of the Radio Signal Processing Laboratory, NTT DoCoMo, where he researched adaptive signal processing, MIMO turbo signal detection, interference cancellation, and space-time coding techniques for broadband mobile communications. In May 2002, he joined the University of Oulu, Finland, where he is a Professor with the Center for the Wireless Communications. Presently, he is serving on the Board of Governors of the IEEE VT Society.

Reiner Thomä (M'93–SM'99) received the Dipl.-Ing. (M.S.E.E.), Dr.-Ing. (Ph.D.E.E.), and the Dr.-Ing. habil. degrees, in electrical engineering (information technology) from Technische Hochschule Ilmenau, Germany, in 1975, 1983, and 1989, respectively.

From 1975 to 1988, he was a Research Associate working in the fields of electronic circuits, measurement engineering, and digital signal processing at the same university. From 1988 to 1990, he was a Research Engineer with the Akademie der Wissenschaften der DDR (Zentrum für Wissenschaftlichen Gerätebau). During this period, he was working in the field of radio surveillance. In 1991, he spent a three-month sabbatical with the University of Erlangen-Nürnberg (Lehrstuhl für Nachrichtentechnik). Since 1992, he has been a Professor of electrical engineering (Electronic Measurement), Technische Universität Ilmenau, and since 1999, he has been the Director of the Institut für Kommunikations- und Meßtechnik at the same university. His research interests include measurement and digital signal processing methods (correlation and spectral analysis, system identification, array methods, time-frequency and cyclostationary signal analysis), their application in mobile radio and radar systems (multidimensional channel sounding, propagation measurement and parameter estimation, ultra-wide-band radar), and measurement based performance evaluation of MIMO transmission systems.

Dr. Thomä is a member of the VDE/ITG, URSI (Comm.A), an elected reviewer of DFG, Chairman of the IEEE Instrumentation and Measurement Society Technical Committee TC-13 "Wireless and Telecommunications," and Chairman of ITG FA 91. "Messverfahren der Informationstechnik."